International Journal of Nanomedicine

Dovepress
open access to scientific and medical research

Open Access Full Text Article

ORIGINAL RESEARCH

SPIONs enhances IL-10-producing macrophages to relieve sepsis via Cav1-Notch1/HES1-mediated autophagy

This article was published in the following Dove Press journal:
International Journal of Nanomedicine

Yujun Xu[1]
Yi Li[1]
Xinghan Liu[1]
Yuchen Pan[1]
Zhiheng Sun[1]
Yaxian Xue[1]
Tingting Wang[1,2]
Huan Dou[1,2]
Yayi Hou[1,2]

[1]The State Key Laboratory of Pharmaceutical Biotechnology, Division of Immunology, Medical School, Nanjing University, Nanjing 210093, People's Republic of China; [2]Jiangsu Key Laboratory of Molecular Medicine, Division of Immunology, Medical School, Nanjing University, Nanjing 210093, People's Republic of China

Background: Sepsis is a life-threatening condition caused by dysregulated host responses to infection. Macrophages, which recognize microbial infections through identification of bacterial markers such as lipopolysaccharide (LPS), are crucial to the pathogenesis of sepsis-associated liver injury. However, the understanding of the SPIONs-mediated modulation of macrophage responses in LPS-induced sepsis and liver injury is limited.

Materials and methods: Superparamagnetic iron oxide nanoparticles (SPIONs) of γ-Fe_2O_3 nanoparticles were prepared, and their morphology and magnetic properties were characterized.

Results: Using a murine model of LPS-induced sepsis and liver injury, we found that SPIONs alleviated LPS-induced sepsis, preventing infiltration of inflammatory cells into the liver. SPIONs also increased the level of interleukin-10 (IL-10) in liver macrophages, while SPIONs's effect on LPS-induced sepsis was abrogated in *IL-10*$^{-/-}$ mice, indicating that the protective effect of SPIONs is dependent on IL-10^{+} macrophages. Moreover, SPIONs activated macrophage autophagy to increase IL-10 production, which was markedly attenuated by autophagy inhibition. Furthermore, SPIONs upregulated the expression of Caveolin-1 (Cav1) in macrophages, which plays a role in cellular uptake of metallic nanoparticles. Interestingly, activation of Cav1 and Notch1/HES1 signaling was involved in SPIONs-induced autophagy in both RAW 264.7 cells and bone marrow-derived macrophages (BMDMs). Our data reveal a novel mechanism for SPIONs -induced autophagy in macrophages, which occurs through activation of the Cav1-Notch1/HES1 signaling pathway, which promotes the production of IL-10 in macrophages, leading to inhibition of inflammation in LPS-induced sepsis and liver injury.

Conclusion: Our results suggest that SPIONs may represent a potential therapeutic agent for the treatment of sepsis and sepsis-induced liver injury.

Keywords: SPIONs, autophagy, IL-10, liver injury, sepsis

Introduction

Sepsis is a major cause of morbidity and mortality for patients in intensive care units worldwide, and the diagnosis and treatment of sepsis are challenging. According to the latest expert consensus on sepsis, it is defined as a life-threatening diagnosis caused by dysregulated host response to infection.[1] Typically, damage caused by infection is effectively controlled by the immune system. However, in some cases, infection may hyperactivate innate host immunity, resulting in an uncontrollable systemic inflammatory response. This uncontrolled, exaggerated

Correspondence: Huan Dou, Yayi Hou
The State Key Laboratory of Pharmaceutical Biotechnology, Division of Immunology, Medical School, Nanjing University, 22 Hankou Road, Nanjing 210093, People's Republic of China
Tel +86 25 8368 6043
Fax +86 25 8368 6043
Email douhuan@nju.edu.cn; yayihou@nju.edu.cn

submit your manuscript | www.dovepress.com
DovePress
http://doi.org/10.2147/IJN.S215055

inflammatory response leads to cell dysfunction and in severe cases, causes multiple organ failure and death. The liver is an important target of sepsis-related injury, and excessive inflammatory reaction leads to liver injury. Effective control of systemic inflammatory progression during the acute phase of sepsis can restore liver homeostasis and prevent sepsis-induced liver injury.[2,3] Unfortunately, the pathogenesis of sepsis and sepsis-induced liver injury is not fully understood, and a new therapeutic scheme is urgently needed.

Macrophages are important innate immune cells, and due to their immunoregulatory function and ubiquitous presence, play important roles in immune homeostasis and the inflammatory process. They are also crucial in the pathogenesis of sepsis and sepsis-associated liver injury. Liver macrophages are generally considered to arise from two sources, liver-resident macrophages and monocyte-derived macrophages. Recent studies demonstrated that activation of liver-resident macrophages leads to the recruitment of innate effector cells to the injured liver. In the hepatic microenvironment, circulation-derived inflammatory monocytes mature into macrophages, potentially contributing to local tissue destruction and resulting in secretion of pro-inflammatory cytokines in the early stages of liver injury.[4,5] In addition, macrophages are the most prominent cell population in liver tissue expressing the immunoregulatory cytokine IL-10.[6] Previously we demonstrated that inhibition of proinflammatory mediators produced by macrophages alleviates experimental sepsis in mice[7,8] and sepsis-induced liver dysfunction by modulating monocyte/macrophage differentiation in acute murine liver failure.[9,10] However, macrophages also play an important role in preventing microbial infection. Thus, it is essential to investigate efficacious modulation of macrophages for the treatment of sepsis and sepsis-induced liver injury.

Autophagy is an innate immune defense mechanism against microbial challenges. Clinical and preclinical studies have indicated that sepsis triggers autophagy in multiple organs, including the liver. Autophagy was also demonstrated to be activated in septic mice followed by subsequent impairment,[11] and the autophagic response is important for regulating lipid metabolism in response to endotoxin challenge.[12] Interestingly, autophagy attenuates inflammation through the induction of cytokines. Moreover, autophagy regulates the inflammasome in macrophages, protecting against liver injury.[13,14] Multiple lines of evidence suggest modulation of macrophages by autophagy might be protective against multiple organ injuries in these murine sepsis models.[15,16] Importantly, autophagy is reportedly related to the Notch signaling pathway in different animal models. Our previous studies demonstrated that the Notch-Hes-1 axis controls TLR7-mediated autophagic death of macrophages via induction of P62.[17] However, the roles of autophagy in the pathogenesis of sepsis remain ill-defined.

Previously, we revealed that SPIONs induces macrophage activation.[18] Of note, SPIONs, which exhibits low cytotoxicity and good biocompatibility, integrates both diagnostic and therapeutic functions. Apart from Ferumoxytol, other types of iron oxide-based synthetic nanoparticles (SPIONs) were investigated. Gu et al showed that multiple endocytic pathways were involved in the internalization process of SPIONs in the RAW264.7 macrophage. They found that the internalized SPIONs were biocompatible.[19] Mou et al showed that SPIO nanoparticles have good superparamagnetic behavior, highly biocompatible characteristics, and are suitable for use in further study of the migratory behavior and biodistribution of dendritic cells in vivo.[20,21] Iversen et al's study demonstrates that accumulation of polyacrylic acid (PAA) coated γ-Fe(2)O(3) NPs (10 mg kg(−1)) does not affect kidney function in healthy mice but temporarily decreases blood pressure.[22] Recently, several nanoparticles have demonstrated significant protective effects against sepsis in preclinical models.[23] Moreover, due to the inherent capacity of their preferential uptake, macrophages process nanoparticles, thereby mediating host inflammatory and immunological responses. Rojas et al found that all SPIONs were internalised and no cell toxicity was observed. SPION treatment in both M2 macrophage models altered their M2 activation profiles, promoted IL-10 production, and stimulated protease-dependent invasion.[24] Interestingly, some evidence suggests that Cav1 is expressed in macrophages. Cav1 over expression inhibits K562 leukemic cell proliferation, promotes endogenous autophagy, and increases the sensitivity of K562 cells to realgar-SPIONs.[25] Thus, it is vital to understand the role of SPIONs in modulating inflammation and autophagy of macrophages in sepsis and sepsis-induced liver injury.

Inflammatory responses occur as a reaction to pathogen recognition receptors detecting various microbial products in innate immune cells. The bacterial endotoxin lipopolysaccharides is a critical factor for inducing systemic inflammatory response and acute tissue injury in some organs, including the liver, during sepsis. In the present

study, we found that SPIONs alleviates liver injury in a murine model of LPS-induced sepsis. Moreover, the effect of SPIONs on LPS-induced septic mice was dependent on IL-10^+ macrophages, and promotion of IL-10-secreting macrophages by SPIONs is mediated by autophagy. Furthermore, SPIONs -induced autophagy was attributed to Cav1-mediated activation of Notch1/HES1 signaling in macrophages. Taken together, our results suggest that SPIONs may represent a potential therapeutic agent for the treatment of sepsis and sepsis-induced liver injury.

Materials and methods

Characterization of SPIONs

SPIONs was provided by Professor Ning Gu's team of Southeast University, Nanjing, China. SPIONs is a nano-iron oxide drug encased by a modified high molecular polymer (polydextrose sorbitol carboxymethyl ether) with good biocompatibility. The structure of iron oxide is γ-Fe_2O_3. High molecular polymers and iron salts were dissolved in ultrapure water, followed by fully and uniformly mixing the two to obtain a uniform solution that was stored in a low temperature environment of −5 to 5 °C. Adding alkali into the mixed solution combined with high-frequency induction heating equipment was used to generate an alternating magnetic field. The external circulating temperature was adjusted to −5 to 15 °C. Next, the high-frequency induction heating equipment external circulation temperature was adjusted to 5–15 °C, followed by raising the temperature of the reaction solution to 80 °C within 30–60 mins. The alternating magnetic field and external circulation were then closed, and various properties of the prepared magnetic nano-iron oxide were characterized using dialysis, ultrafiltration and filtration of the reaction solution to determine hydration particle size, iron core size, iron core crystal structure, saturation magnetization and magnetic susceptibility.

Reagents and antibodies

Baf-A1, Notch signal inhibitor-(DAPT) and LPS were purchased from Sigma (St. Louis, MO, USA). Anti-LC3 monoclonal (#12741), anti-BECN1 (#3495), anti-Cav1 (#3267), anti-Notch1 (#3608), and anti-HES1 (#11988) antibodies were from Cell Signaling (Boston, MO, USA). Anti-F4/80(ab6640) monoclonal antibodies were from Abcam (Cambridge, MA, USA).

Cell culture

RAW 264.7 cells were obtained from the Shanghai Institute of Cell Biology (Shanghai, China). Cells were cultured in DMEM medium (Gibco, Carlsbad, CA) with 10% fetal bovine serum (Gibco, Carlsbad, CA). For generation of mouse BMDMs, cells were obtained from 8-week-old female C57BL/6 mice. Cells were cultivated in RPM1640 medium (Gibco) supplemented with 50 ng/mL M-CSF (PEPROTECH, Rocky Hill, USA), antibiotics and 10% FBS. Medium was replaced on day 3, and cells were collected and used for experiments on day 5. All cell lines were incubated at 37 °C in a humidified environment with 5% CO_2.

Small interfering RNAs (SiRNAs) and Cav1 overexpression

SiRNAs targeting Cav1 and HES1 were purchased from Ribobio (Guangzhou, China). RAW 264.7 cells were transfected with 100 nM siRNA or non-targeting siRNA controls using Lipofectamine 2000 reagent (Invitrogen) according to the manufacturer's instructions. For over-expression of Cav1, RAW 264.7 cells were transfected with a Cav1 expression plasmid from Genechem (Shanghai, China) using Lipofectamine 2000 reagent (Invitrogen) according to the manufacturer's instructions. RAW 264.7 cells were transfected with siRNAs or plasmids for 24 h and then stimulated with SPIONs for 24 h. siRNA sequences were as follows: non-targeting control siRNA; 5′-ACGUGA CACGUUCGGAGAAUU-3′; Cav1:5′-AUCCCAUCCAG AGUUGCUUGUGAUC-3′; HES1: 5′-TGTCATCCAGCT TACATCTCACAC-3′. *Cav1* or *HES1* mRNA and protein expression levels were assessed by qRT-PCR and Western blot, respectively.

GFP-LC3 stable cell lines and quantitative GFP-LC3 analyses

RAW 264.7-GFP-LC3 stable cell line was established by transient transfection of GFP-LC3 plasmid using Lipofectamine 2000 reagent (Invitrogen). RAW 264.7-GFP-LC3 stable cell lines were transfected with individual siRNAs or plasmids or were treated with SPIONs. GFP-LC3 puncta formation was determined by capturing images using an Olympus FV1000 confocal microscope (Olympus, Tokyo, Japan).

RNA isolation and qRT-PCR

Total RNA was extracted from tissues and cultured cells using TRIzol Reagent (Invitrogen, USA) according to the manufacturer's instructions. A total of 1 μg RNA was used as a template for single strand cDNA synthesis. Q-PCR for GAPDH and SiRNAs was performed on an ABI Step One Plus Detection System (Applied Biosystems, USA) using SYBR green dye (Bio-Rad, USA). Reaction conditions were 95 °C for 10 min followed by 40 cycles of 95 °C for 15 s, 60 °C for 30 s, and 72 °C for 30 s. All reactions were run in triplicate. The gene expression levels were normalized to GAPDH. The primer sequences are listed in Table S1.

Western blotting

Tissue or cells were lysed in buffer containing 50 mM Tris-Cl pH 8.0, 150 mM NaCl, 0.02% NaN3, 0.1% SDS, 100 mg/mL phenyl-methylsufonyl fluoride (PMSF), 1 mg/mL Aprotinin, 1% Triton. 10 μg/mL aprotinin, 10 μg/mL leupeptin, and 1 mM dithiothreitol. 1 mM para-nitrophenyl phosphate, and 0.1 mM Na_3VO_4 were added as protease and phosphatase inhibitors, respectively. After centrifugation, protein samples were subjected to 10% SDS-PAGE and transferred onto PVDF membranes (Roche, Mannheim, Germany). Membranes were blocked in TBST (1 mM Tris-HCl, pH 7.4, 150 mM NaCl, 0.05% Tween-20) containing 5% BSA for 1.5 h and subsequently incubated overnight at 4 °C with diluted primary antibodies against proteins of interest. All antibodies were used at a dilution of 1:1,000 unless otherwise specified.

Mice

Animal studies were approved by the Medical School for Animal Use and Care Committee of Nanjing University in accordance with guidelines of the US NIH. Six to eight weeks old male C57BL/6 mice and 6–8 weeks old male *IL-10*$^{-/-}$ mice were purchased from the Model Animal Research Center of Nanjing University. Mice were reared under Specific Pathogen Free conditions at a temperature of 24 °C and provided standard rodent chow and water. Mice were administered intraperitoneal (i.p.) LPS injection (5 mg/kg) for 4 h followed by treatment with SPIONs (4 mg/kg) through the vena caudalis. Twenty hours after SPIONs injection, mice were euthanized. Livers were harvested, and he total iron levels were detected using atomic absorption spectrometry (AAS) analysis.

Flow cytometry analysis

Liver cells were obtained based on methods described by Nemeth et al Briefly, freshly removed liver tissues were minced into small pieces and incubated in RPMI 1640 medium with 300 U/mL collagenase type I (Sigma), 300 U/mL collagenase type IV (Sigma) and 50 U/mL DNase I (Sigma). After incubation, cell suspensions were filtered through a 70-um cell strainer and then washed with complete RPMI medium. Single-cell suspensions were incubated with an Fc receptor blocker (CD16/32, eBioscience) to reduce nonspecific antibody binding. The panel of antibodies used in these experiments included CD11b-APC, F4/80-FITC, IL-10 PE (all from eBioscience), CD4-FITC, CD25-APC and Foxp3-PE (all from Biolegend). Among these antibodies, CD11b, F4/80, CD4 and CD25 cause cell surface staining, while IL-10 and foxp3 result in both cell surface and intracellular staining. Flow cytometry was performed using a FACS Calibur flow cytometer (BD Bioscience), and data were analyzed using FlowJo software (TreeStar, Ashland, OR).

Atomic absorption spectroscopy

Cultured cells or tissues prepared for measuring Fe concentration were lysed using aqua regia and qualified using an atomic absorption spectroscopy graphite furnace (Hitachi 180-80, Japan) according to the standard curve for Fe.

H&E staining

Fresh liver tissues were fixed in 4% PFA (pH 7.4) and gradually dehydrated, embedded in paraffin, cut into 3 μm sections and stained with hematoxylin and eosin for light microscopy. Scores were evaluated based on the presence of epithelial hyperplasia, mononuclear infiltrate and polymorphonuclear infiltrate (0= none; 1= mild; 2= moderate; 3= severe)

Immunofluorescence

Liver tissues were collected for immunofluorescence staining to assess LC3B and macrophage localization. Briefly, 8 μm-thick frozen liver slices were fixed in cold methanol/acetone (1:1) for 10 min at −20 °C. Following three extensive washings with PBS, samples were blocked with 3% bovine serum albumin (BSA) in PBS for 60 min at room temperature followed by incubation with anti-F4/80 and anti-LC3B primary antibodies at a 1:200 dilution for 2 h. After rinsing three times in PBS, samples were incubated with Alexa Fluor 488-conjugated secondary antibody at a 1:400 dilution for 1.5 h at room temperature in the dark, and then nuclei were stained using

DAPI. Slides were visualized using a Nikon Eclipse Ti-U fluorescence microscope equipped with a digital camera (DS-Ri1, Nikon).

ELISA

The protein levels of IL-6, TNF-α, and IL-10 in mouse serum were detected using the corresponding mouse enzyme-linked immunosorbent assay (ELISA) kit according to the manufacturer's instructions (Biolegend, China).

Statistical analysis

Statistical analysis was performed using Prism 6 (GraphPad Software). Statistical significance was evaluated by unpaired Student's *t*-test. Correlation

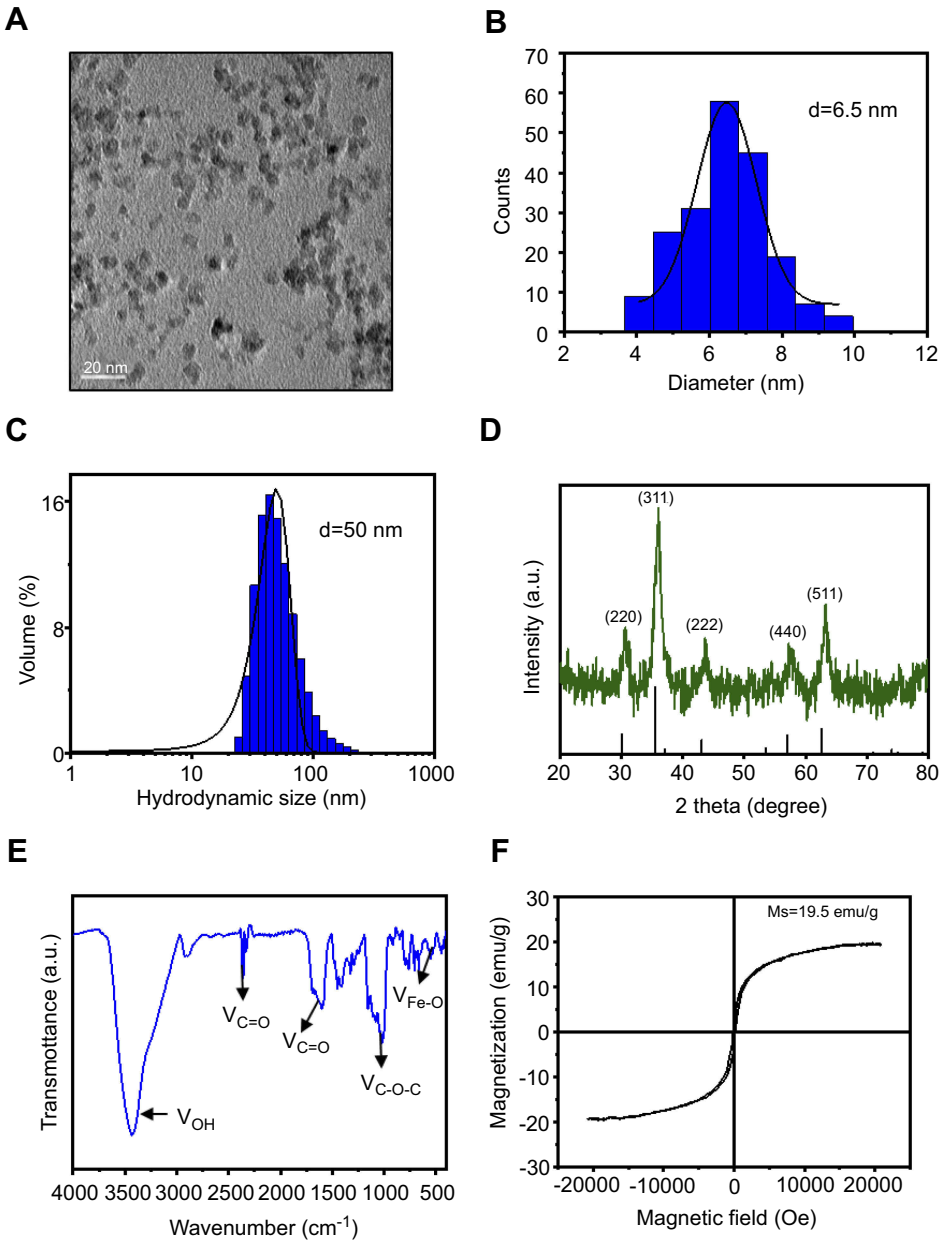

Figure 1 Construction of SPIONs. (**A**) TEM images and size distribution of SPIONs. (**B**) The average diameter of SPIONs was calculated from TEM images (histogram in the center). (**C**) DLS size of SPIONs in water. (**D**) XRD of SPIONs. Diffraction peaks of the magnetite phase of the iron oxide were used to assign planar indices. (**E**) FT-IR spectra of SPIONs marked with the characteristic peaks. (**F**) Magnetic hysteresis loops of SPIONs.

Abbreviations: SPIONS, superparamagnetic iron oxide nanoparticles; TEM, transmission electron microscopy; DLS, dynamic light scattering; XRD, X-ray diffraction; VSM, Vibrating Sample Magnetometer; FT-IR, Fourier Transform Infrared.

significance was determined using linear regression. Differences with p-values ≤0.05 were considered statistically significant.

Results

Characterization of SPIONs

Morphology and size of SPIONs were observed using transmission electron microscopy (TEM) (Figure 1A). The average core size of SPIONs was 6.5 nm (Figure 1B). The average hydrodynamic diameter of SPIONs for three batches determined by dynamic light scattering (DLS) was 50±2.2 nm (Figure 1C). Powder X-ray diffraction (XRD) patterns SPIONs are shown in Figure 1D. XRD analysis indicated that SPIONs exhibits five distinct diffraction peaks: 220, 311, 222, 440 and 511. Specifically, the band in the Fourier transform infrared spectrum (Figure 1E) from 3200 cm^{-1} to 3400 cm^{-1} corresponds to the OH stretching vibration. The sharp COO− specific stretching vibration peak presented at 1610 cm^{-1}, and multiple peaks around 1500 cm^{-1} shifted to around 1440 cm^{-1}, indicating that COO− chelates with Fe ion. Furthermore, the absorption peak at 580 cm^{-1} was attributed to SPIONs. To characterize its magnetic properties, SPIONs with different coatings was analyzed, and the magnetization curves obtained using a Vibrating Sample Magnetomet (VSM) are shown in Figure 1F. SPIONs showed a smooth M-H curve at ambient temperature, and saturation magnetization values of SPIONs were 19.5 emu/g.

SPIONs alleviates liver injury in a murine model of LPS-induced sepsis

Sepsis is caused by bacterial infection. The endotoxin LPS is a critical factor for inducing systemic inflammatory response and acute tissue injury on some organs, including the liver, during sepsis. We examined the therapeutic effects of SPIONs using a murine model of LPS-induced sepsis. Compared to the PBS group, the levels of total iron were reduced in LPS-challenged animals. SPIONs treatment reverses iron loss in response to LPS (Figure 2B). Moreover, we examined liver histopathology. Histological assessment of liver sections from mice with LPS-induced sepsis revealed marked evidence of edema, increased inflammatory cell infiltration, and severe hemorrhage, while SPIONs significantly attenuated these signs of liver damage Figure 2C. In addition, liver damage markers, aspartate aminotransferase (AST) and alanine aminotransferase (ALT), were markedly increased in the serum of LPS-induced septic mice, while SPIONs significantly decreased the serum levels of these liver enzymes. Of note, no differences were observed between SPIONs-treated non-septic mice and control non-septic mice (Figure 2D). These results suggest that SPIONs alleviates liver injury in septic mice, potentially through restoration of dysregulated iron homeostasis.

SPIONs induces macrophage IL-10 expression

Macrophages are not only involved in iron-regulating processes but also play essential roles throughout all phases of sepsis. In the hepatic microenvironment, macrophage-related immune responses are associated with local tissue destruction and secretion of pro-inflammatory cytokines. In the liver of LPS-induced septic mice, the number of $CD11b^{+}F4/80^{+}$macrophage was markedly increased, whereas administration of SPIONs reduced the macrophage population (Figure 2E). No significant change in the macrophage population was detected in SPIONs-treated normal mice compared to normal mice. Moreover, in serum of LPS-induced septic mice, concentrations of interleukin-6 (IL-6) and tumor necrosis factor-α (TNF-α) were significantly increased, while SPIONs treatment attenuated their levels (Figure 2G). Most noteworthy, SPIONs significantly increased serum IL-10 level in the LPS-induced sepsis model.

Macrophages are thought to contribute to the state of tolerance through their expression of IL-10 in response to LPS and bacteria. Interestingly, our results showed that SPIONs significantly increased the number of IL-10 producing macrophages in the liver tissue of LPS-induced septic mice compared to LPS-induced septic mice that were not treated with SPIONs (Figure 2F). Regulatory T (Treg) cells act as critical negative regulators of inflammation in various biological contexts, and their negative regulatory function is closely related with the expression of transforming growth factor (TGF–β), IL-10 and other cytokines.[26] To verify whether Treg cells are involved in increased IL-10 expression in this murine sepsis model, the number of $Foxp3^{+}$ Treg cells was assessed by flow cytometry. We found the increase of Il-10 is not caused by Treg cells (Figure S1A).

These data indicate that SPIONs treatment not only improves iron loss from the liver but also enhances

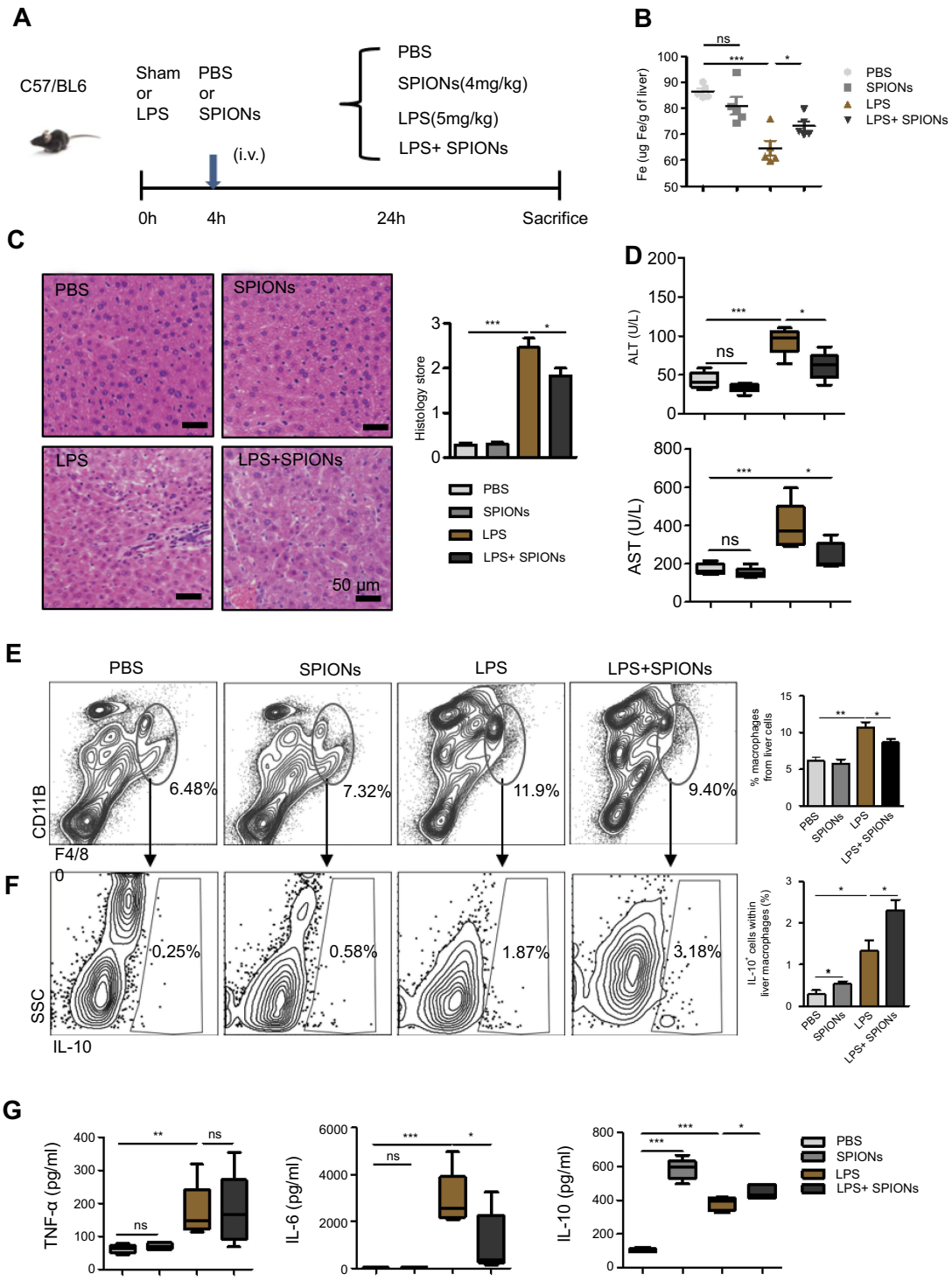

Figure 2 SPIONs reduces liver injury in LPS-induced sepsis via a subset of macrophages. (**A**) Mice were injected intraperitoneally with PBS and LPS (5 mg/kg) via a tail vein injection with SPIONs (4 mg/kg) or not injected (controls). After 24 hrs, mice were euthanized, and livers were removed from each mouse (n=6 for each group). (**B**) Mouse liver tissue containing free Fe and whole livers, treated as indicated, were lysed using aqua regia, and total Fe was qualified using an atomic absorption spectroscopy graphite furnace. (**C**) Histological analysis of livers was visualized by H&E staining. Livers were microscopically analyzed and histologically scored by a pathologist. (**D**) Levels of ALT and AST were detected in the sera of PBS mice, SPIONs-treated mice or LPS mice from SPIONs-treated or untreated mice. (**E**) Flow cytometry data of hepatic cells stained with antibodies for CD11b and F4/80 are presented. The proportion of macrophages is presented. (**F**) The proportion of IL-10^{+} producing macrophages in PBS mice, SPIONs-treated mice or LPS mice from SPIONs-treated or untreated mice was determined by flow cytometry. (**G**) The concentration of blood inflammatory cytokines (TNF-a, IL-6) and anti-inflammatory cytokines (IL-10) was measured by ELISA. Data with error bars are presented as the mean ± SD. Each panel is a representative experiment of at least three independent biological replicates. Scale bars, 50 mm. *p<0.05, **p<0.01, ***p<0.001 as determined by unpaired Student's t-test.

Abbreviations: SPIONS, superparamagnetic iron oxide nanoparticles; LPS, lipopolysaccharide; PBS, phosphate buffer saline; AST, aspartate aminotransferase; ALT, alanine aminotransferase; IL-6, interleukin-6; TNF-α, tumor necrosis factor-α; IL-10, interleukin-10; ns, not significant.

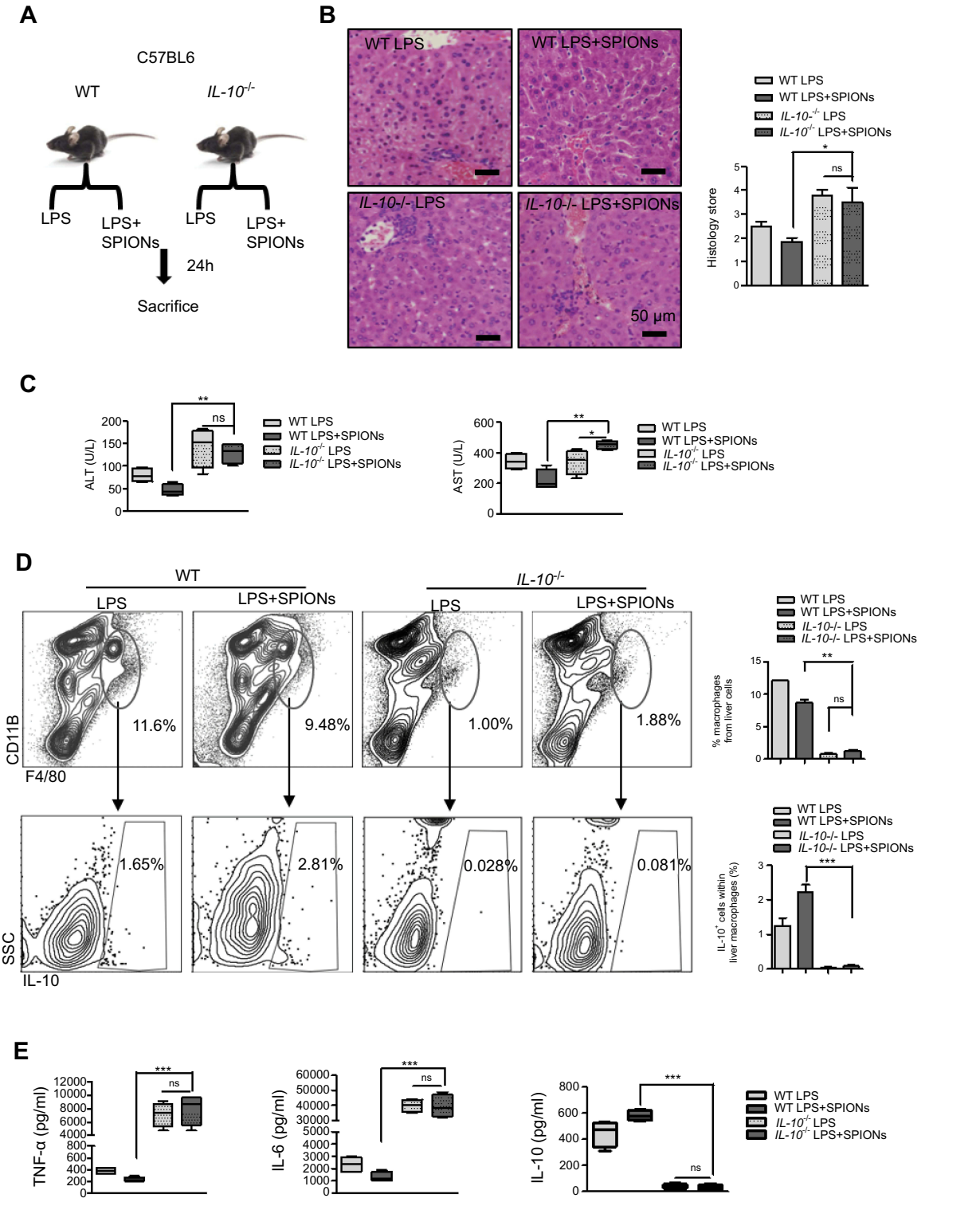

Figure 3 IL-10^{+} is necessary for SPIONs to suppress LPS-induced sepsis. (**A**) WT mice and *IL-10*$^{-/-}$mice (n=6 for each group) were injected intraperitoneally with LPS (5 mg/kg) or a tail vein injection of SPIONs (4 mg/kg). After 24 hrs, mice were euthanized, and their livers were removed. (**B**) Histological analysis of livers is visualized by H&E staining. Livers were microscopically analyzed. Histological scores were assigned by a pathologist. (**C**) The levels of ALT and AST were detected in the sera of LPS induced WT and *IL-10*$^{-/-}$ mice for SPIONs treated and untreated mice. (**D**) Flow cytometry data of hepatic cells stained with antibodies for CD11b and F4/80 are presented. The proportion of IL-10^{+} producing macrophages was determined by flow cytometry. (**E**) Concentrations of blood inflammatory cytokines (TNF-a, IL-6) and anti-inflammatory cytokines (IL-10) were measured by ELISA. Data with error bars are presented as the mean±SD. Each panel is a representative experiment of at least three independent biological replicates. Scale bars, 50 mm. *p<0.05, **p<0.01, ***p<0.001 as determined by unpaired Student's t-test.

Abbreviations: SPIONS, superparamagnetic iron oxide nanoparticles; LPS, lipopolysaccharide; PBS, phosphate buffer saline; FBS, fetal bovine serum; AST, aspartate aminotransferase; ALT, alanine aminotransferase; IL-6, interleukin-6; TNF-α, tumor necrosis factor-α; IL-10, interleukin-10; ns, not significant.

immunosuppression of macrophages in LPS-induced septic mice, suggesting that SPIONs-induced IL-10 expression by macrophages may be essential to relieve liver injury in LPS-induced sepsis.

SPIONs's alleviation of LPS-induced sepsis is dependent on IL-10+ macrophages

To determine the role of IL-10 in sepsis, LPS-induced sepsis was established in *IL-10*$^{-/-}$ mice (Figure 3A). Histological analysis showed that IL-10 deficiency reduced the effect of SPIONs on inflammatory infiltration and hepatic hemorrhage (Figure 3B). The serum ALT and AST levels were remarkably increased in LPS-induced *IL-10*$^{-/-}$ mice. As anticipated, SPIONs treatment did not decrease the levels of ALT or AST in LPS-induced *IL-10*$^{-/-}$ mice compared with those of LPS-induced WT mice (Figure 3C). Moreover, LPS caused a marked increase in the total number of macrophages in *IL-10*$^{-/-}$ mice compared to WT mice. SPIONs treatment did not significantly change cell populations in LPS-induced sepsis in *IL-10*$^{-/-}$ mice compared to LPS-induced sepsis in WT mice (Figure 3D). SPIONs also did not change IL-10-producing macrophage in LPS-treated *IL-10*$^{-/-}$ mice compared to LPS-treated WT mice (Figure 3D). Nevertheless, when Foxp3+ cells in WT and IL-10$^{-/-}$ mice were examined by flow cytometry, similar changes in the number of Foxp3+ cells were observed between IL-10$^{-/-}$ and WT mice treated with LPS or LPS+SPIONs (Figure S2A). Moreover, LPS induced a significant progressive increase of inflammatory cytokines (IL-6 and TNF-a) in *IL-10*$^{-/-}$mice, while SPIONs treatment did not reduce the cytokine levels (Figure 3E). Taken together, these data indicate that SPIONs's actions on LPS-induced septic mice is dependent on IL-10.

Promotion of IL-10-secreting macrophages by SPIONs is related to autophagy

Our findings confirmed that SPIONs significantly promotes macrophage secretion of the anti-inflammatory factor IL-10. To investigate how SPIONs affects macrophage inflammatory responses, we measured the mRNA levels of *TNF-α, iNOS, IL-10* and *Arg-1* in the mouse macrophage RAW 264.7 cell line treated with SPIONs (200 μg/mL) or LPS (100 ng/mL) for 24 h. The results showed that SPIONs effectively upregulates expression of *IL-10* (Figure 4A) but not *TNF-α, iNOS* or *Arg-1* (Figure S3A-C). SPIONs also more effectively increased the mRNA and protein levels of IL-10 compared to LPS alone (Figure 4A and B). Notably, flow cytometry analysis revealed that SPIONs also up-regulates IL-10^{+} macrophage in both RAW 264.7 cells and BMDMs (Figure 4C and D).

Autophagy reportedly attenuates inflammation through the induction of cytokines, such as IL-10.[27–29] To explore whether autophagy is involved in IL-10 production by macrophages, RAW 264.7 cells or BMDMs were treated with the autophagy inhibitor Baf-A1 for 2 h followed by SPIONs stimulation. As shown in Figure 4E and F, IL-10^{+} cell populations were remarkably reduced in Baf-A1-treated cells compared with Baf-A1-untreated cells. Moreover, the Notch1/HES1 signaling pathway is tightly associated with autophagic response. We next assessed whether Notch activity also controls IL-10 protein processing in macrophages treated with SPIONs. As shown in Figure S3D and E, compared to control cells (SPIONs stimulation only), DAPT, an indirect inhibitor of the Notch pathway, pre-treated cells exhibited decreased IL-10^{+} cell populations in both RAW 264.7 cells and BMDMs. These data suggest that SPIONs enhances IL-10 secretion through activation of autophagy in macrophages, and Notch1/HES1 may be critical for macrophage production of the anti-inflammatory factor IL-10.

SPIONs triggers autophagy in macrophages

To determine whether SPIONs induces autophagy in macrophages, RAW 264.7 cells were treated with 10 μg/mL, 50 μg/mL and 200 μg/mL SPIONs for 6 h, 12 h and 24 h, respectively. A shift from LC3I to LC3II was observed in SPIONs-treated RAW 264.7 cells compared to control cells using Western blot (Figure 5A and B). Increased LC3II/LC3I ratio indicates that SPIONs induced autophagy in RAW 264.7 cells in a time- and dose-dependent manner. Moreover, SPIONs also upregulated Beclin1 expression in RAW 264.7 cells (Figure 5A and C). To assess whether increased LC3II was localized to the autophagosome membrane, RAW 264.7 cells were stably transfected with GFP-LC3 stably expressing fusion proteins and were then treated with SPIONs for 24 hrs. The results showed that SPIONs increases LC3II puncta (Figure 5D and E), a critical marker of autophagy, in macrophages. These data confirm that SPIONs does indeed induce autophagy in RAW 264.7 cells.

If expression of LC3II increases in the presence of a lysosome inhibitor, it suggests increased autophagic flux. By contrast, if the LC3II levels remain unaltered, it is possible that autophagosome accumulation is due to the blockade of autophagy flux. To further reveal the effect of SPIONs on autophagy flux in macrophages, the autophagy

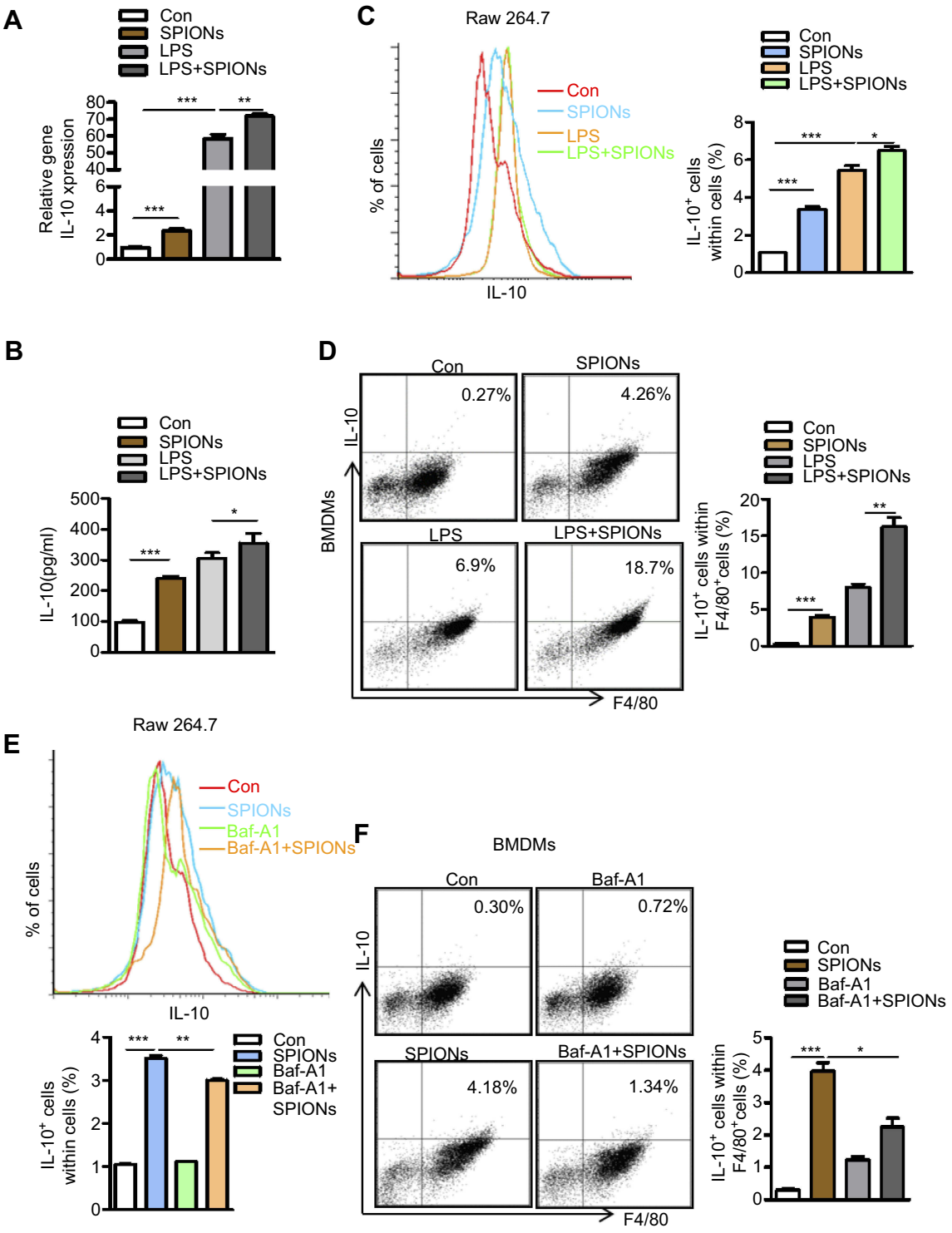

Figure 4 SPIONs promotes IL-10-secreting macrophages to undergo autophagy. (**A**) mRNA expression of IL-10 in RAW 264.7 cells pre-treated with LPS (100 ng/mL) for 2 h followed by no stimulation or stimulation with 200 μg/mL SPIONs for 24 h. (**B**) IL-10 in culture supernatants was measured by ELISA assays. (**C, D**) Proportion of IL-10$^+$ cells in RAW 264.7 cells and BMDMs cells was determined by flow cytometry. (**E, F**) The percentage of IL-10$^+$ cells in RAW 264.7 cells and BMDMs pre-treated with the Baf-A1 (10 μM) for 2 h followed by no stimulation or stimulation with 200 μg/mL SPIONs for 24 h was determined by flow cytometry. Data with error bars are presented as the mean ± SD. Each panel is a representative experiment of at least three independent biological replicates. *p<0.05, **p<0.01, ***p<0.001 as determined by unpaired Student's t-test.

Abbreviations: SPIONS, superparamagnetic iron oxide nanoparticles; LPS, lipopolysaccharide; IL-10, interleukin-10; Baf-A1, Bafilomycin A1.

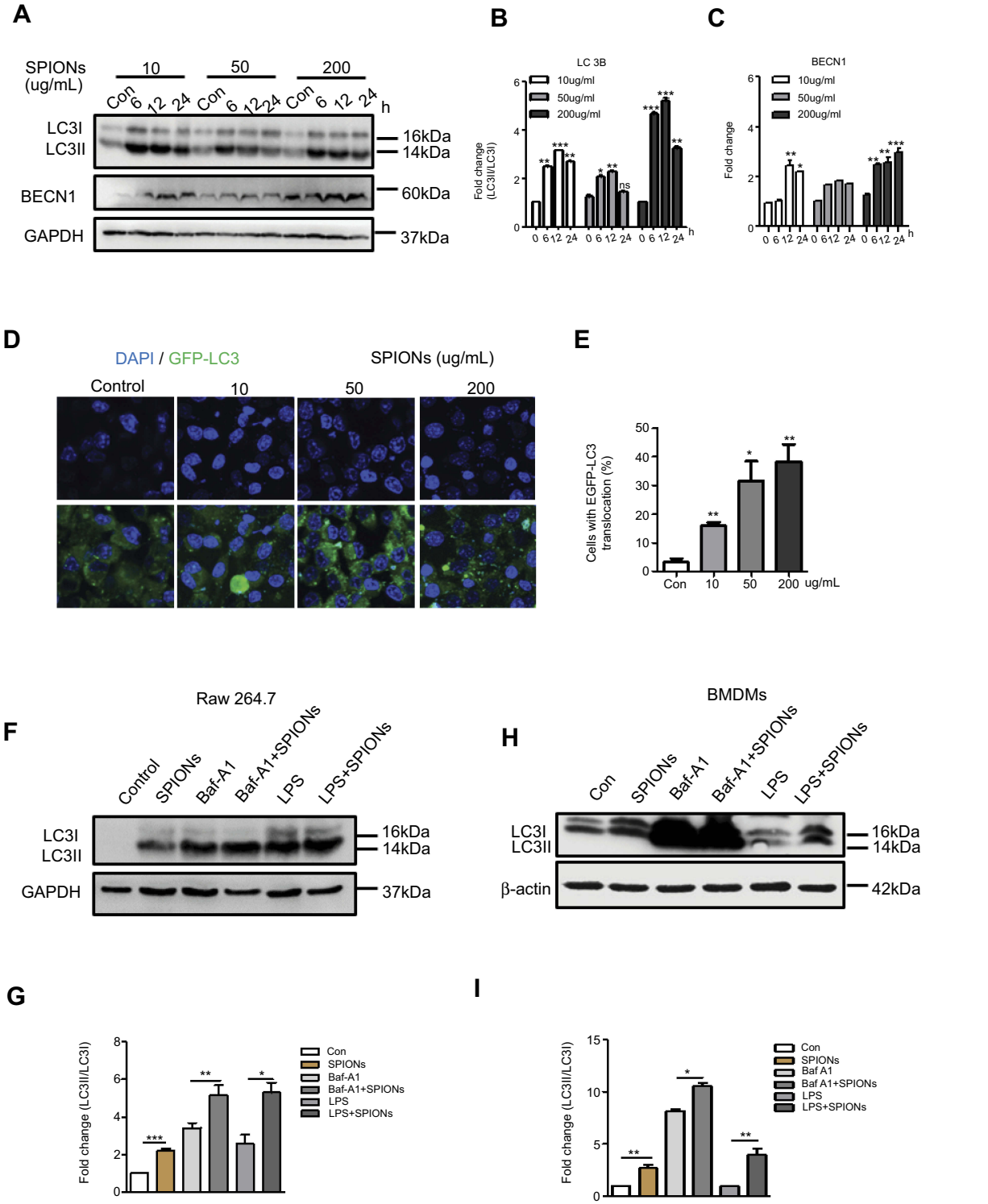

Figure 5 SPIONs triggers autophagy in macrophages. (**A**) Protein levels of LC3II and BECN-1 in RAW 264.7 cells stimulated with 10 μg/mL, 50 μg/mL or 200 μg/mL SPIONs measured at 0, 6, 12, and 24 h. (**B, C**) Density of LC3II:LC3I and BECN-1 bands in each group was quantified and normalized to GAPDH expression. (**D**) RAW 264.7 cells were transfected with GFP-LC3 plasmids and treated with 10 μg/mL, 50 μg/mL or 200 μg/mL SPIONs for 24 hrs. Confocal immunofluorescent staining of GFP-LC3 (green) and nuclear DAPI staining (blue) in cells. (**E**) Number of LC3 puncta per cell quantified by confocal microscopy. (**F**) RAW264.7 cells were pre-treated with the autophagy inhibitor BafA1 (10 μM) or LPS (100 ng/mL) for 2 h followed by treatment with SPIONs (200 μg/mL) for 24 h. Immunoblot of LC3 in cells. (**G**) Normalized values for LC3II expression are indicated in the above Western blot bands (**F**). (**H**) BMDMs were pre-treated with the autophagy inhibitor BafA1 (10 μM) or LPS (100 ng/mL) for 2 h and followed by treatment with SPIONs (200 μg/mL) for 24 h Protein expression of LC3II was detected by Western blot. (**I**) Density of LC3II:LC3I bands in each group was quantified. Data with error bars are presented as the mean ± SD. Each panel is a representative experiment of at least three independent biological replicates. *p<0.05, **p<0.01, ***p<0.001 as determined by unpaired Student's t-test.

Abbreviations: SPIONS, superparamagnetic iron oxide nanoparticles; IL-10, interleukin-10; Baf-A1, Bafilomycin A1; LC3B, light chain 3B; BECN1, Beclin 1; DAPI, 4′, 6-diamidino-2-phenylindole; BMDMs, bone marrow derived macrophage cells.

inhibitor Baf-A1 was used during SPIONs treatment. As shown in Figure 5F, Baf-A1-treated RAW264.7 cells showed higher transformation of LC3II in response to SPIONs than treatment with BafA1 alone. These results suggest that autophagosome accumulation might be attributed to autophagy induction by SPIONs since LPS induces autophagy in both primary human macrophages and the murine macrophage RAW 264.7 cell line. RAW 264.7 cells treated with SPIONs/LPS showed higher levels of LC3II compared to the SPIONs group or LPS group (Figure 5F and G). Of note, similar changes were also detected in BMDMs (Figure 5H and I). Taken together, these results demonstrate that SPIONs induces significant accumulation of autophagosomes in macrophages under an inflammatory environment.

Cav1 is critical for SPIONs-induced autophagy in macrophages

Cav1, the principal structural component of caveolae, has been reported to play a role in ceramic particles cellular uptake.[30,31] Furthermore, Cav1 is associated with the autophagic process in septic mice. Therefore, we hypothesized that Cav1 may be critical for the uptake of SPIONs and subsequent autophagic induction in macrophages. We first assessed the effect of SPIONs on the expression of Caveolin family members in macrophages. RAW 264.7 cells treated with 200 μg/mL SPIONs for 24 h showed significantly increased *Cav1* expression, but expression of *Cav2* and *Cav3* was unchanged (Figure S4A). Western blot and immunofluorescence results also revealed that SPIONs markedly enhanced Cav1 expression in a time-dependent manner (Figure 6A and B, Figure S4B). Moreover, RAW 264.7 cells were transfected with Cav1 plasmids for 24 h followed by treatment with SPIONs for 24 h. The transfection efficiency was measured, and the results showed Cav1 expression in RAW 264.7 cells was upregulated at both the mRNA and protein levels (Figure S4C and D). As expected, over expression of Cav1 significantly increased LC3II expression at the protein level (Figure 6C) and GFP-LC3 puncta (Figure 6D) in RAW 264.7 cells. Next, we assessed the effects of downregulation of Cav1 expression in RAW 264.7 cells using specific siRNA, and silencing efficiency is shown in Figure S4E and F. Knockdown of Cav1 markedly reduced both LC3II accumulation and LC3 puncta in autophagosomes in RAW 264.7 cells (Figure 6E–G, Figure S4G–I) in response to SPIONs. These results indicate that Cav1 participates in SPIONs-induced autophagy in macrophages.

To determine the effect of Cav1 on uptake of SPIONs by macrophages, RAW 264.7 cells were transfected with Cav1 plasmids or si-Cav1, and total iron was measured after treatment with SPIONs for 24 hrs. Knockdown of Cav1 markedly reduced uptake of SPIONs, while over expression of Cav1 elevated the uptake of SPIONs (Figure 6H). These data suggest that Cav1 is involved in the uptake of SPIONs by macrophages.

SPIONs-induced autophagy is attributed to Cav1-mediated activation of the Notch1/HES1 pathway in macrophages

Recent studies imply that the Notch signaling pathway is involved in regulating neuronal differentiation of stem cells and that Cav1 coordinates and couples with Notch1 in neural stem cells.[32,33] In addition, Notch signaling regulates autophagy and promotes macrophage activation.[34–36] Previously, we demonstrated that Notch signaling is involved in autophagic death of macrophages in mice with lupus.[17] However, the interactive role of Cav1 and Notch signaling in macrophages is unknown. To investigate the mechanism of SPIONs-induced autophagy in macrophages, the expression pattern of Notch receptors in RAW 264.7 cells was measured. The results showed that SPIONs significantly increased the expression of *Notch1* but not *Notch2, Notch3*, or *Notch4* (Figure 7A). SPIONs also upregulated the mRNA level of *HES1* (Figure 7B). Moreover, both real-time PCR and Western blot results revealed that SPIONs stimulation markedly enhanced Notch1 expression in a time-dependent manner (Figure S5A–D).

To confirm the role of Notch1 signaling in SPIONs-induced autophagy, RAW 264.7 cells were treated with the Notch signaling inhibitor DAPT at 5 μM, 10 μM and 50 μM for 2 h before SPIONs treatment. DAPT significantly inhibited the protein expression level of Notch1 (Figure 7C). Compared with SPIONs-induced RAW 264.7 cells, DAPT decreased the levels of LC3II (Figure 7C, Figure S5E) and LC3 puncta (Figure 7G). Specifically, DAPT also reduced he protein level of LC3II induced by SPIONs (Figure 7D, Figure S5F). HES1 is the best-characterized target gene of Notch signaling. To determine whether HES1 is involved in SPIONs-induced autophagy, RAW 264.7 cells were transfected using three independent siRNAs against HES1 for 24 h. As expected, knockdown of HES1 was correlated with decreased LC3II accumulation

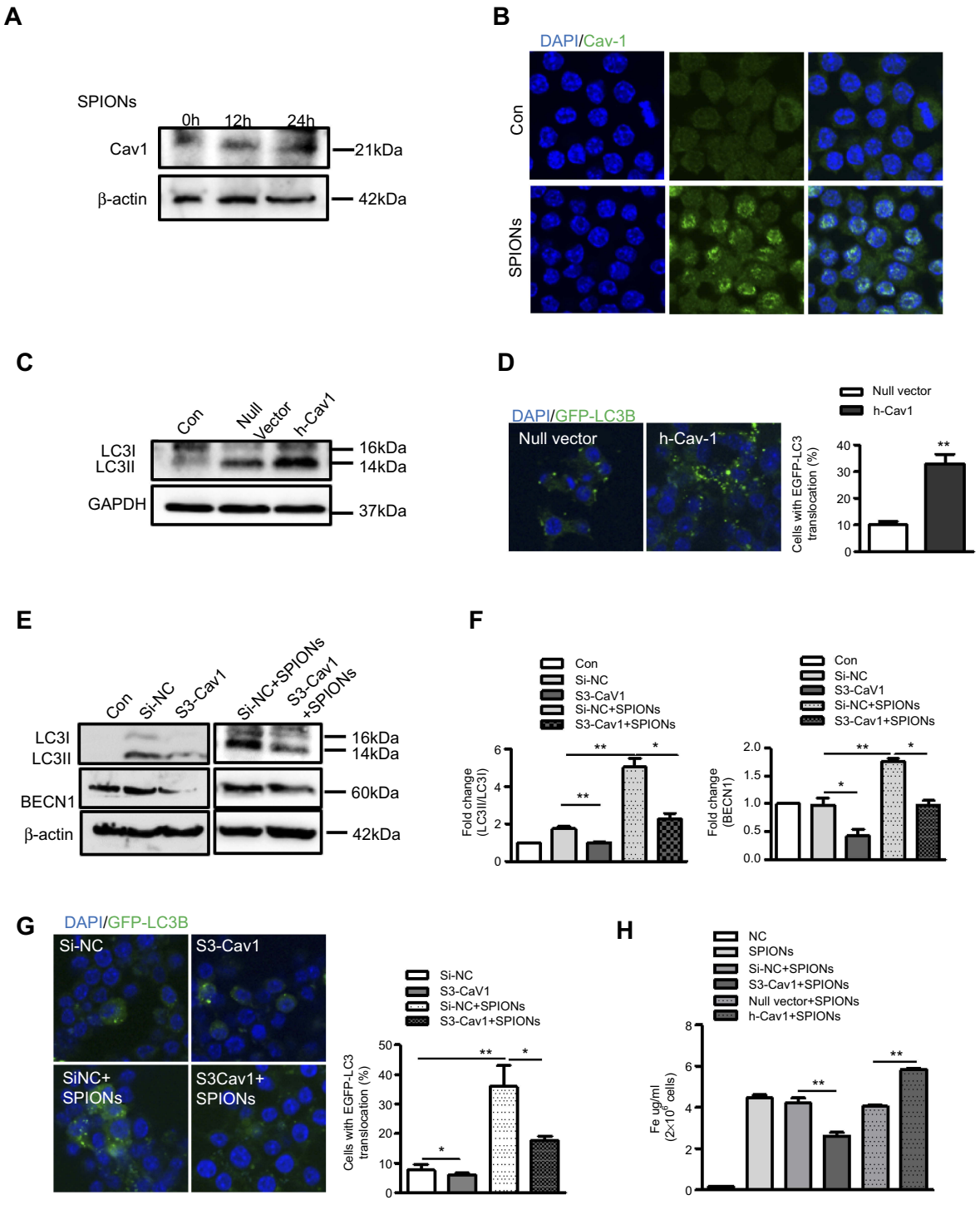

Figure 6 Cav1 mediates SPIONs-induced autophagy in macrophages. (**A**) Immunoblotting analysis showing expression of Cav1 in RAW 264.7 cells not stimulated or stimulated with 200 μg/mL SPIONs for 24 h. Density of Cav1 bands was quantified and normalized to β-actin. (**B**) Immunofluorescent analysis of Cav1 (green) and nuclear DAPI (blue) followed by processing for confocal microscopy. (**C**) The protein expression levels of LC3II were detected by Western blot in RAW 264.7 cells transfected with Cav1 plasmids for 24 h. Density of Cav1 bands was quantified and normalized to GAPDH. (**D**) Confocal immunofluorescent staining of GFP-LC3 (green) and nuclear DAPI staining (blue) in RAW264.7 cells transfected with GFP-LC3 plasmids and treated with Cav1 plasmid for 24 h. Number of LC3 puncta per cell was quantified by confocal microscopy. (**E, F**) Immunoblotting analysis of LC3I, LC3II and BECN1 in RAW 264.7 cells transfected with Si-Cav1 for 24 h and then stimulated with SPIONs for 24 h. LC3II:LC3I ratio and BECN-1 were normalized to β-actin (**G**) Fluorescent images of RAW 264.7 cells transfected with GFP-LC3 plasmids followed by treatment with Si-Cav1 for 24 h and subsequent stimulation with SPIONs for 24 h. LC3-II puncta (green) were observed by confocal microscopy. (**H**) Total Fe was quantified using an atomic absorption spectroscopy graphite furnace in RAW 264.7 cells transfected with Cav1 plasmid or Si-Cav1 followed by stimulation with SPIONs for 24 h. Data with error bars are presented as the mean ± SD. Each panel is a representative experiment of at least three independent biological replicates. *p<0.05 and **p<0.01as determined by unpaired Student's t-test.

Abbreviations: SPIONS, superparamagnetic iron oxide nanoparticles; LPS, lipopolysaccharide; Baf-A1, Bafilomycin A1; LC3B, light chain 3B; BECN1, Beclin 1; Cav1, Caveolin-1; DAPI, 4′, 6-diamidino-2-phenylindole; BMDMs, bone marrow derived macrophage cells.

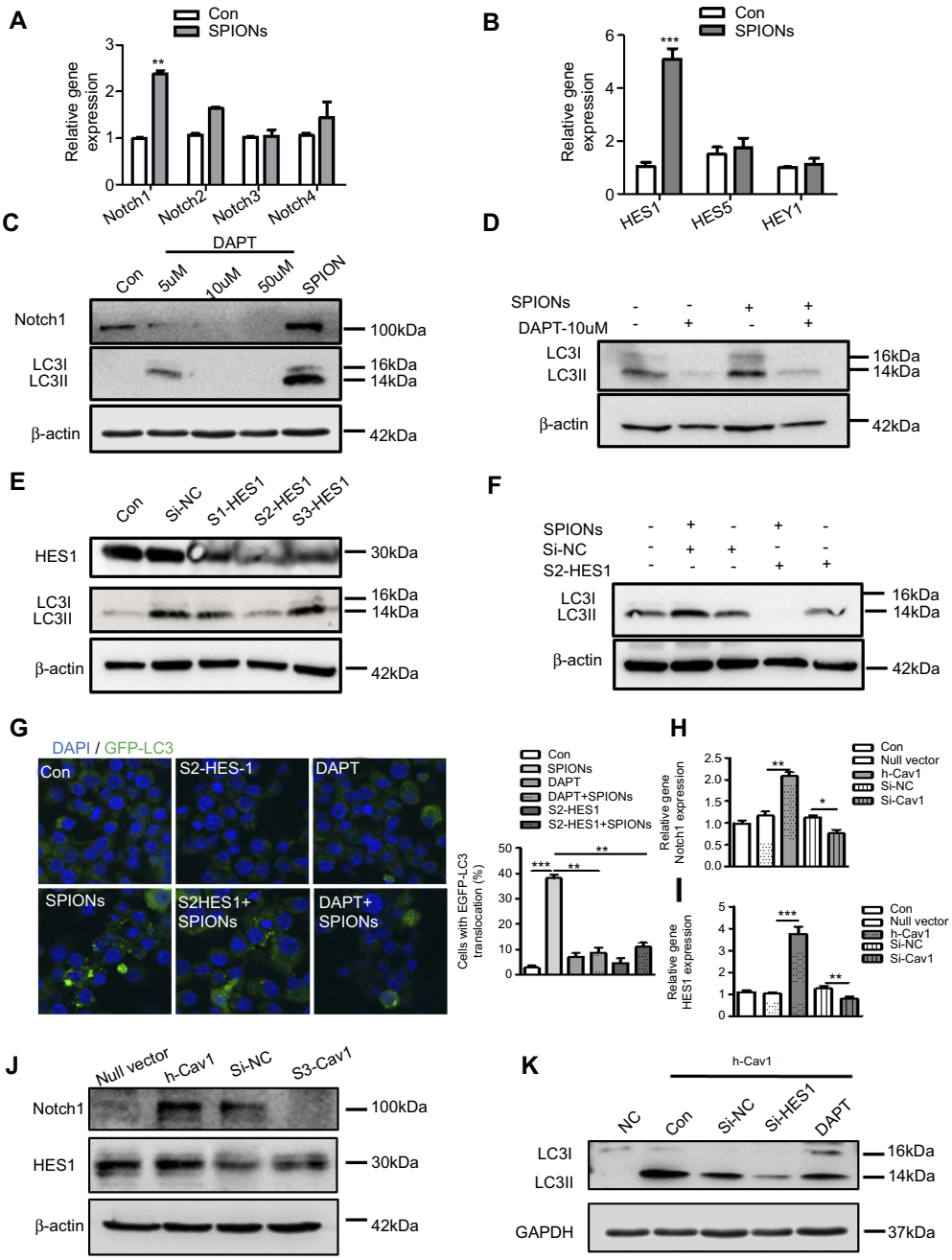

Figure 7 Cav1-mediated autophagy of macrophages is activated via Notch1/HES1 signaling. (**A, B**) mRNA expression of Notch receptors, HES1, HES5 and HEY1, in RAW 264.7 cells treated with 200 μg/mL SPIONs for 24 h. (**C**) Expression of Notch1 and LC3II in RAW 264.7 cells treated with DAPT (5 μM, 10 μM and 50 μM) and 200 μg/mL SPIONs for 24 h by immunoblotting. (**D**) Expression of LC3II in RAW 264.7 cells pre-treated with DAPT (10 μM) for 2 h followed by 200 μg/mL SPIONs stimulation for 24 h by immunoblotting. (**E**) RAW 264.7 cells were transfected with Si-HES1 for 24 h. The protein levels of HES1 and LC3II were assessed by Western blot. (**F**) RAW 264.7 cells were pre-treated with Si-HES1 for 24 h and then stimulated with 200 μg/mL SPIONs for 24 h. The protein levels of LC3II were assessed by Western blot. (**G**) Fluorescent images of RAW 264.7 cells transfected with GFP-LC3 plasmids followed by transfection with Si-HES1or DAPT (10 μM) were stimulated with SPIONs for 24 h. LC3II puncta (green) were observed by confocal microscopy (DAPI, blue). (**H, I**) mRNA expression of Notch1 and HES1 in RAW 264.7 cells transfected with Si-Cav1 or Cav1 plasmid for 24 h. (**J**) Expression of Notch1 and HES1 in RAW 264.7 cells transfected with si-Cav1 or Cav1 plasmid for 24 h by immunoblotting. (**K**) Expression of LC3II in RAW 264.7 cells transfected with Si-HES1or DAPT (10 μM) followed by transfection with Cav1 plasmid for 24 h by immunoblotting. Data with error bars are presented as the mean ± SD. Each panel is a representative experiment of at least three independent biological replicates. *p<0.05, **p<0.01, ***p<0.001 as determined by unpaired Student's t-test.
Abbreviations: SPIONS, superparamagnetic iron oxide nanoparticles; LC3B, light chain 3B; BECN1, Beclin 1; Cav1, Caveolin-1; DAPI, 4′, 6-diamidino-2-phenylindole.

Figure 7E and G, Figure S5G). In HES1-knockdown RAW 264.7 cells, SPIONs-induced increases in LC3II accumulation and punctate GFP-LC3 were attenuated (Figure 7F and G, Figure S5H).

To verify the relationship between Cav1 and Notch1-HES1 signaling, we used real-time PCR and Western blot to analyze Notch1 and HES1 in RAW 264.7 cells in response to manipulating Cav1 expression. As shown in

Figure 7H–J and Figure S5I, Cav1 inhibition in cells significantly reduced the mRNA and protein levels of Notch1 and HES1, while Cav1 over-expressing increased the Notch1 and HES1 levels. Furthermore, RAW 264.7 cells were transfected with Si-HES1 or administered DAPT (10 μM) for 24 h followed by transfection with Cav1 plasmids for 24 h. The protein level of LC3II was assessed by Western blot. The results showed that inhibition of HES1 or Notch1 significantly reduced the protein level of LC3II, which were not reversed by over-expression of Cav1 (Figure 7K, Figure S5J). Taken together, these data indicate that upregulation of Cav1 activates Notch1/HES1 signaling, leading to autophagy in macrophages.

Autophagy of SPIONs-induced macrophage occurs in liver injury in LPS-induced septic mice

The above findings indicate that SPIONs-induced autophagy is attributed to Cav1-mediated activation of the Notch1/HES1 pathway, which promotes IL-10 production in macrophages in vitro. To determine the results of in vitro experiments, Cav1, Notch1/HES1 and specific markers of autophagy were detected in macrophages from liver tissue of LPS-induced septic mice. Using immunofluorescence with an anti-LC3B antibody, we found that SPIONs induced significantly increased LC3B in F4/80 positive macrophages both in PBS and LPS-treated mice. Nevertheless, SPIONs significantly enhanced LC3B expression of F4/80 positive macrophages in liver tissue of LPS-induced septic mice (Figure 8A and B). Western blot results also illustrate that SPIONs upregulated LC3II expression in liver tissues of LPS-induced septic mice (Figure 8C). Moreover, SPIONs remarkably upregulated the protein and mRNA levels of Cav1, Notch1 and HES1 in liver tissue of LPS-induced septic mice (Figure 8D and E). Together, these data demonstrate that SPIONs promotes the development of autophagy in liver tissue macrophages, suggesting Cav1-Notch1/HES1-mediated autophagy may be involved in SPIONs's therapeutic effect on liver injury in LPS-induced sepsis.

Discussion

Sepsis is now defined as life-threatening organ dysfunction caused by a dysregulated host response to infection. The liver is the primary target organ in sepsis, and sepsis patients develop severe liver injury, which progresses to liver failure.[1–3] In recent years, SPIONs has been proposed for use in sepsis diagnostics and treatment.[37–39] In this study, we used SPIONs (γ-Fe_2O_3), have high biocompatibility. SPIONs were prepared, and their morphology and magnetic properties were characterized. We found that SPIONs significantly ameliorated the symptoms of sepsis and liver injury as shown by decreased levels of ALT and AST, including decreased expression of pro-inflammatory cytokines TNF-a and IL-6 and increased expression of the anti-inflammatory cytokine IL-10. SPIONs increased IL-10 expression in liver macrophages. Moreover, IL-$10^{-/-}$ mice experienced significantly aggravated liver injury and exacerbation of inflammation. We examined the liver macrophage response in LPS-sepsis mice exposed to SPIONs and found that treatment with LPS caused a marked increase in the population of macrophages ($CD11b^{+}F4/80^{+}$). By contrast, the macrophages population was reduced in SPIONs-treated LPS mice. Indeed, Song et al have recently shown that IL-10 is involved in the immune dysfunction in splenic lymphocytes from septic animals, as reflected by their decreased ability to release IL-2 and IFN. Furthermore, the role of IL-10 in depressing monocyte function in sepsis was recently demonstrated. Our results showed that SPIONs elevates the number of IL-10 producing macrophages in LPS-induced mice, while IL-10 deficiency blocked hepatic injury remission induced by SPIONs. In addition, IL-10 deficiency did not cause a significant change in the number of macrophages in liver tissues. IL-10 can be produced by Treg cells, and we found a marked increase in populations of $FoxP3^{+}$ Treg cells in the liver of LPS-induced septic mice but observed no difference in the presence or absence of SPIONs (Figure S1). Moreover, a similar change in $FoxP3^{+}$ Treg cells was observed in the liver of IL-$10^{-/-}$ mice. SPIONs clearly affects secretion of IL–10 by macrophages during sepsis (Figure S2). These data suggest that the protective effect of SPIONs on LPS-induced sepsis may be dependent on IL-10^{+} macrophages.

Autophagy is activated in early stages of sepsis, inhibiting pathological development, and increasing autophagy attenuates organ damage.[40,41] We speculate that autophagy may be related to the involvement of macrophages in sepsis. We demonstrated that SPIONs-induced autophagy was critical for increasing macrophages expression of IL-10. SPIONs increased the levels of LC3B in mouse liver macrophages. SPIONs also markedly induced both the secretion of IL-10 and autophagy in RAW 264.7 cells

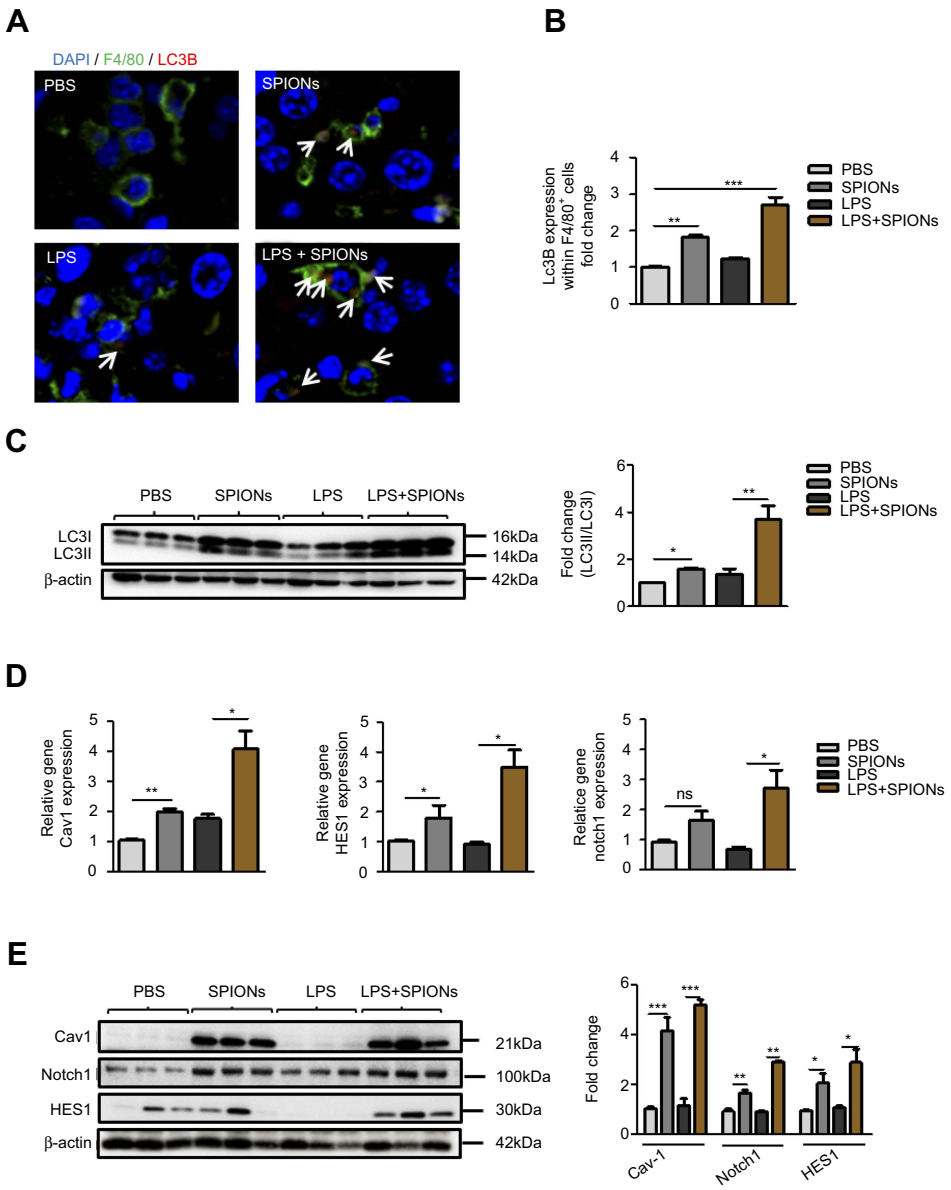

Figure 8 SPIONs-induced autophagy in macrophage in response to liver injury of LPS-induced septic mice. (**A, B**) Confocal immunofluorescent staining of F4/80 (green), autophagy marker LC3B (red, indicated by arrows) and nuclear DAPI (blue) in liver tissue of PBS mice, SPIONs-treated mice or LPS mice from SPIONs-treated or untreated mice. (**C**) Levels of LC3II were examined in liver tissues by Western blot. Density of LC3II:LC3I bands in each group was quantified. (**D**) mRNA expression of Cav1, Notch1 and HES1 in liver cells was detected using qPCR. (**E**) Immunoblotting analysis of Cav1, Notch1 and HES1 in mouse liver cells. Quantification of Cav1, Notch1 and HES1 band density normalized to GAPDH. Data with error bars are presented as the mean ± SD. Each panel is a representative experiment of at least three independent biological replicates. Scale bars, 50 mm. *p<0.05, **p<0.01, ***p<0.001 as determined by unpaired Student's t-test.

Abbreviations: SPIONS, superparamagnetic iron oxide nanoparticles; LPS, lipopolysaccharide; LC3B, light chain 3B; Cav1, Caveolin-1; DAPI, 4′, 6-diamidino-2-phenylindole; ns, not significant.

and BMDMs in vitro. By contrast, inhibition of autophagy by Baf-A1 reduced expression of IL-10 in macrophages. Thus, it seems reasonable to infer that SPIONs promotes IL-10-secreting macrophages, which is related to their autophagy in LPS-induced septic mice.

Cav1 plays an essential role in regulating various cellular signaling pathways and exerts an important function in immune cell responses. Recently, several studies have shown that Cav1 is involved in the autophagic process.[25,42–44] Cav1 is also expressed in macrophages.[45,46] We found that Cav1 mediates macrophage uptake of SPIONs and enhances autophagy to protect against septic liver injury. Notch signaling plays a key role in the induction of autophagy,[47] regulating cell differentiation, proliferation, and survival.[48] Notch signaling also modulates cytokine production in

T lymphocytes and macrophages.[49,50] In our study, SPIONs increased the protein levels of Notch1 and HES1 in macrophages, while the lack of Cav1 or inhibition of Notch/HES1 signaling prevented SPIONs from effectively enhancing the LC3B autophagosome levels in cells. Moreover, SPIONs increased Cav1 expression, while Cav1 inhibition using siRNA reduced expression and activation of Notch1. Furthermore, SPIONs increased the activation of autophagy via Cav1-Notch1/HES1, which was illustrated both in vitro and vivo. These data indicate that SPIONs-induced autophagy is attributed to Cav1-mediated activation of Notch1/HES1 signaling in macrophages.

However, it is worth discussing whether the influence of SPIONs on liver macrophages is related to their size and is clear. From previous studies,[51–53] SPIONs can affect the biological functions of macrophages. Moreover, Chen et al explored the cytotoxicity and mechanisms of the synthesized SPIONs with different size distributions of 30, 80 and 120 nm, and compared their potential capability in inducing IL-1β release in mouse bone marrow-derived macrophages (BMMs). They found that SPIONs induced IL-1β release in a size- and dose-dependent manner.[54] Furthermore, by varying the surface hydrophobicity of the SPIONs with a core size around 10 nm, the more hydrophobic surface ligand attracted proteins with higher surface hydrophobicity and formed a more dynamic corona. The stably bound proteins could significantly enhance cellular uptake of SPIONs.[55] In our present study, although there is no direct evidence that SPIONs can be degraded by macrophages in liver and spleen, it is possible our SPIONs will be cleared by macrophage in some ways.

Conclusion

In summary, we demonstrated a novel mechanism of SPIONs-induced autophagy in macrophages through activation of the Cav1-Notch1/HES1 signal pathway, which promotes the production of IL-10 in macrophages, leading to the inhibition of inflammation in an LPS-induced sepsis and liver injury model. Our results suggest that SPIONs may be a potential therapeutic agent for the treatment of sepsis and sepsis-induced liver injury.

Abbreviations

SPIONs, Superparamagnetic iron oxide nanoparticles; TEM, transmission electron microscopy; DLS, dynamic light scattering; XRD, X-ray diffraction; VSM, Vibrating Sample Magnetometer; FT-IR, Fourier Transform Infrared; LPS, lipopolysaccharide; PBS, phosphate buffer saline; FBS, fetal bovine serum; AST, aspartate aminotransferase; ALT, alanine aminotransferase; IL-6, interleukin-6; TNF-α, tumor necrosis factor-α; IL-10, interleukin-10; Baf-A1, Bafilomycin A1; LC3B, light chain 3B; BECN1, Beclin 1; Cav1, Caveolin-1; DAPI, 4′, 6-diamidino-2-phenylindole; BMDMs, bone marrow derived macrophages; DAPT, N-[N-(3,5-Difluorophenacetyl)-L-alanyl]-S-phenylglycine t-butyl Ester; M-CSF, Macrophage Colony-stimulating Factor.

Acknowledgments

This work was supported by National Key Research and Development Program of China (2017YFA0104303) and grants from the National Natural Science Foundation of China (No. 91542113). We are grateful to Prof. Ning Gu from Southeast University for providing us with the SPIONs.

Author contributions

All authors contributed to data analysis, drafting and revising the article, gave final approval of the version to be published, and agree to be accountable for all aspects of the work.

Disclosure

The authors report no conflicts of interest in this work.

References

1. Singer M, Deutschman CS, Seymour CW, et al. The Third International consensus definitions for sepsis and septic shock (Sepsis-3). *JAMA*. 2016;315(8):801–810. doi:10.1001/jama.2016.0287
2. Savio LEB, de Andrade Mello P, Figliuolo VR, et al. CD39 limits P2X7 receptor inflammatory signaling and attenuates sepsis-induced liver injury. *J Hepatol*. 2017;67(4):716–726. doi:10.1016/j.jhep.2017.05.021
3. Chen X, Cai X, Le R, et al. Isoliquiritigenin protects against sepsis-induced lung and liver injury by reducing inflammatory responses. *Biochem Biophys Res Commun*. 2018;496(2):245–252. doi:10.1016/j.bbrc.2017.11.159
4. Antoniades CG, Quaglia A, Taams LS, et al. Source and characterization of hepatic macrophages in acetaminophen-induced acute liver failure in humans. *Hepatology*. 2012;56(2):735–746. doi:10.1002/hep.25657
5. Brempelis KJ, Crispe IN. Infiltrating monocytes in liver injury and repair. *Clin Transl Immunol*. 2016;5(11):e113. doi:10.1038/cti.2016.62
6. Knolle PA, Loser E, Protzer U, et al. Regulation of endotoxin-induced IL-6 production in liver sinusoidal endothelial cells and Kupffer cells by IL-10. *Clin Exp Immunol*. 1997;107(3):555–561. doi:10.1046/j.1365-2249.1997.d01-959.x
7. Dou H, Song Y, Liu X, et al. A novel benzenediamine derivate rescued mice from experimental sepsis by attenuating proinflammatory mediators via IRAK4. *Am J Respir Cell Mol Biol*. 2014;51(2):191–200. doi:10.1165/rcmb.2013-0411OC

8. Gong W, Hu E, Dou H, et al. A novel 1,2-benzenediamine derivative FC-99 suppresses TLR3 expression and ameliorates disease symptoms in a mouse model of sepsis. *Br J Pharmacol*. 2014;171(21):4866–4878. doi:10.1111/bph.12797
9. Terashima-Hasegawa M, Ashino T, Kawazoe Y, Shiba T, Manabe A, Numazawa S. Inorganic polyphosphate protects against lipopolysaccharide-induced lethality and tissue injury through regulation of macrophage recruitment. *Biochem Pharmacol*. 2019;159:96–105. doi:10.1016/j.bcp.2018.11.017
10. Zhao Y, Zhu H, Wang H, et al. FC-99 ameliorates sepsis-induced liver dysfunction by modulating monocyte/macrophage differentiation via Let-7a related monocytes apoptosis. *Oncotarget*. 2018;9(19):14959–14976. doi:10.18632/oncotarget.24127
11. Ho J, Yu J, Wong SH, et al. Autophagy in sepsis: degradation into exhaustion? *Autophagy*. 2016;12(7):1073–1082. doi:10.1080/15548627.2016.1179410
12. Chung KW, Kim KM, Choi YJ, et al. The critical role played by endotoxin-induced liver autophagy in the maintenance of lipid metabolism during sepsis. *Autophagy*. 2017;13(7):1113–1129. doi:10.1080/15548627.2017.1319040
13. Ding WX, Jaeschke H. Autophagy in macrophages regulates the inflammasome and protects against liver injury. *J Hepatol*. 2016;64(1):16–18. doi:10.1016/j.jhep.2015.10.003
14. Ilyas G, Zhao E, Liu K, et al. Macrophage autophagy limits acute toxic liver injury in mice through down regulation of interleukin-1beta. *J Hepatol*. 2016;64(1):118–127. doi:10.1016/j.jhep.2015.08.019
15. Ueno T, Komatsu M. Autophagy in the liver: functions in health and disease. *Nat Rev Gastroenterol Hepatol*. 2017;14(3):170–184. doi:10.1038/nrgastro.2016.185
16. Zhou S, Gu J, Liu R, et al. Spermine alleviates acute liver injury by inhibiting liver-resident macrophage pro-inflammatory response through ATG5-dependent autophagy. *Front Immunol*. 2018;9:948. doi:10.3389/fimmu.2018.00948
17. Li X, Liu F, Zhang X, et al. Notch-Hes-1 axis controls TLR7-mediated autophagic death of macrophage via induction of P62 in mice with lupus. *Cell Death Dis*. 2016;7(8):e2341. doi:10.1038/cddis.2016.244
18. Zhao J, Zhang Z, Xue Y, et al. Anti-tumor macrophages activated by ferumoxytol combined or surface-functionalized with the TLR3 agonist poly (I: C) promote melanoma regression. *Theranostics*. 2018;8(22):6307–6321. doi:10.7150/thno.29746
19. Gu J, Xu H, Han Y, et al. The internalization pathway, metabolic fate and biological effect of superparamagnetic iron oxide nanoparticles in the macrophage-like RAW264.7 cell. *Sci China Life Sci*. 2011;54(9):793–805. doi:10.1007/s11427-011-4215-5
20. Mou Y, Chen B, Zhang Y, et al. Influence of synthetic superparamagnetic iron oxide on dendritic cells. *Int J Nanomedicine*. 2011;6:1779–1786. doi:10.2147/IJN.S23240
21. Mou Y, Hou Y, Chen B, et al. In vivo migration of dendritic cells labeled with synthetic superparamagnetic iron oxide. *Int J Nanomedicine*. 2011;6:2633–2640. doi:10.2147/IJN.S24307
22. Iversen NK, Frische S, Thomsen K, et al. Superparamagnetic iron oxide polyacrylic acid coated gamma-Fe2O3 nanoparticles do not affect kidney function but cause acute effect on the cardiovascular function in healthy mice. *Toxicol Appl Pharmacol*. 2013;266(2):276–288. doi:10.1016/j.taap.2012.10.014
23. Yuk SA, Sanchez-Rodriguez DA, Tsifansky MD, Yeo Y. Recent advances in nanomedicine for sepsis treatment. *Ther Deliv*. 2018;9(6):435–450. doi:10.4155/tde-2018-0009
24. Rojas JM, Sanz-Ortega L, Mulens-Arias V, Gutierrez L, Perez-Yague S, Barber DF. Superparamagnetic iron oxide nanoparticle uptake alters M2 macrophage phenotype, iron metabolism, migration and invasion. *Nanomedicine*. 2016;12(4):1127–1138. doi:10.1016/j.nano.2015.11.020
25. Shi D, Liu Y, Xi R, et al. Caveolin-1 contributes to realgar nanoparticle therapy in human chronic myelogenous leukemia K562 cells. *Int J Nanomedicine*. 2016;11:5823–5835. doi:10.2147/IJN.S115158
26. Jin RM, Warunek J, Wohlfert EA. Therapeutic administration of IL-10 and amphiregulin alleviates chronic skeletal muscle inflammation and damage induced by infection. *ImmunoHorizons*. 2018;2(5):142–154. doi:10.4049/immunohorizons.1800024
27. Petrovski G, Zahuczky G, Majai G, Fesus L. Phagocytosis of cells dying through autophagy evokes a pro-inflammatory response in macrophages. *Autophagy*. 2007;3(5):509–511. doi:10.4161/auto.4731
28. Wang Y, Li YB, Yin JJ, et al. Autophagy regulates inflammation following oxidative injury in diabetes. *Autophagy*. 2013;9(3):272–277. doi:10.4161/auto.23628
29. Zhong Z, Sanchez-Lopez E, Karin M. Autophagy, inflammation, and immunity: a Troika governing cancer and its treatment. *Cell*. 2016;166(2):288–298. doi:10.1016/j.cell.2016.05.051
30. Chatterjee M, Ben-Josef E, Robb R, et al. Caveolae-mediated endocytosis is critical for albumin cellular uptake and response to albumin-bound chemotherapy. *Cancer Res*. 2017;77(21):5925–5937. doi:10.1158/0008-5472.CAN-17-0604
31. Chen D, Monteiro-Riviere NA, Zhang LW. Intracellular imaging of quantum dots, gold, and iron oxide nanoparticles with associated endocytic pathways. *Wiley Interdiscip Rev Nanomed Nanobiotechnol*. 2017;9(2):e1419. doi:10.1002/wnan.1419
32. Campos LS, Decker L, Taylor V, Skarnes W. Notch, epidermal growth factor receptor, and beta1-integrin pathways are coordinated in neural stem cells. *J Biol Chem*. 2006;281(8):5300–5309. doi:10.1074/jbc.M511886200
33. Yanjie J, Jiping S, Yan Z, Xiaofeng Z, Boai Z, Yajun L. Effects of Notch-1 signalling pathway on differentiation of marrow mesenchymal stem cells into neurons in vitro. *Neuroreport*. 2007;18(14):1443–1447. doi:10.1097/WNR.0b013e3282ef7753
34. Eun HS, Jeong WI. Dual Notch signaling in proinflammatory macrophage activation. *Hepatology*. 2016;63(4):1381–1383. doi:10.1002/hep.28386
35. Xu J, Chi F, Guo T, et al. NOTCH reprograms mitochondrial metabolism for proinflammatory macrophage activation. *J Clin Invest*. 2015;125(4):1579–1590. doi:10.1172/JCI76468
36. Zhang C, Li W, Wen J, Yang Z. Autophagy is involved in mouse kidney development and podocyte differentiation regulated by Notch signalling. *J Cell Mol Med*. 2017;21(7):1315–1328. doi:10.1111/jcmm.13061
37. Soh M, Kang DW, Jeong HG, et al. Ceria-zirconia nanoparticles as an enhanced multi-antioxidant for sepsis treatment. *Angewandte Chemie*. 2017;56(38):11399–11403. doi:10.1002/anie.201704904
38. Thamphiwatana S, Angsantikul P, Escajadillo T, et al. Macrophage-like nanoparticles concurrently absorbing endotoxins and proinflammatory cytokines for sepsis management. *Proc Natl Acad Sci U S A*. 2017;114(43):11488–11493. doi:10.1073/pnas.1714267114
39. van der Poll T, van de Veerdonk FL, Scicluna BP, Netea MG. The immunopathology of sepsis and potential therapeutic targets. *Nat Rev Immunol*. 2017;17(7):407–420. doi:10.1038/nri.2017.36
40. Amer AO. The many uses of autophagosomes. *Autophagy*. 2013;9(5):633–634. doi:10.4161/auto.24146
41. von Muhlinen N, Thurston T, Ryzhakov G, Bloor S, Randow F. NDP52, a novel autophagy receptor for ubiquitin-decorated cytosolic bacteria. *Autophagy*. 2010;6(2):288–289. doi:10.4161/auto.6.2.11118
42. Liu Y, Wang Y, Shi D, Zou W. [Autophagy and caveolin-1 in cancer: a review]. *Chin J Biotechnol*. 2012;28(8):912–917.
43. Chen Z, Nie SD, Qu ML, et al. The autophagic degradation of Cav-1 contributes to PA-induced apoptosis and inflammation of astrocytes. *Cell Death Dis*. 2018;9(7):771. doi:10.1038/s41419-018-0795-3
44. Chen ZH, Cao JF, Zhou JS, et al. Interaction of caveolin-1 with ATG12-ATG5 system suppresses autophagy in lung epithelial cells. *Am J Physiol Lung Cell Mol Physiol*. 2014;306(11):L1016–L1025. doi:10.1152/ajplung.00268.2013
45. Hiromura M, Nohtomi K, Mori Y, et al. Caveolin-1, a binding protein of CD26, is essential for the anti-inflammatory effects of dipeptidyl peptidase-4 inhibitors on human and mouse macrophages. *Biochem Biophys Res Commun*. 2018;495(1):223–229. doi:10.1016/j.bbrc.2017.11.016

46. Ning P, Gao L, Zhou Y, et al. Caveolin-1-mediated endocytic pathway is involved in classical swine fever virus Shimen infection of porcine alveolar macrophages. *Vet Microbiol*. 2016;195:81–86. doi:10.1016/j.vetmic.2016.09.016
47. Zou M, Hu C, You Q, Zhang A, Wang X, Guo Q. Oroxylin A induces autophagy in human malignant glioma cells via the mTOR-STAT3-Notch signaling pathway. *Mol Carcinog*. 2015;54(11):1363–1375. doi:10.1002/mc.22212
48. Fortini ME. Notch signaling: the core pathway and its posttranslational regulation. *Dev Cell*. 2009;16(5):633–647. doi:10.1016/j.devcel.2009.03.010
49. Foldi J, Chung AY, Xu H, et al. Autoamplification of Notch signaling in macrophages by TLR-induced and RBP-J-dependent induction of Jagged1. *Journal of Immunol*. 2010;185(9):5023–5031. doi:10.4049/jimmunol.1001544
50. Outtz HH, Wu JK, Wang X, Kitajewski J. Notch1 deficiency results in decreased inflammation during wound healing and regulates vascular endothelial growth factor receptor-1 and inflammatory cytokine expression in macrophages. *Journal of Immunol*. 2010;185(7):4363–4373. doi:10.4049/jimmunol.1000720
51. Shi M, Cheng L, Zhang Z, Liu Z, Mao X. Ferroferric oxide nanoparticles induce prosurvival autophagy in human blood cells by modulating the Beclin 1/Bcl-2/VPS34 complex. *Int J Nanomedicine*. 2015;10:207–216.
52. Wu Q, Jin R, Feng T, et al. Iron oxide nanoparticles and induced autophagy in human monocytes. *Int J Nanomedicine*. 2017;12:3993–4005. doi:10.2147/IJN.S135189
53. Zhang X, Zhang H, Liang X, et al. Iron oxide nanoparticles induce autophagosome accumulation through multiple mechanisms: lysosome impairment, mitochondrial damage, and ER stress. *Mol Pharm*. 2016;13(7):2578–2587. doi:10.1021/acs.molpharmaceut.6b00405
54. Chen S, Chen S, Zeng Y, et al. Size-dependent superparamagnetic iron oxide nanoparticles dictate interleukin-1beta release from mouse bone marrow-derived macrophages. *J Appl Toxicol*. 2018;38(7):978–986. doi:10.1002/jat.3606
55. Ashby J, Pan S, Zhong W. Size and surface functionalization of iron oxide nanoparticles influence the composition and dynamic nature of their protein corona. *ACS Appl Mater Interfaces*. 2014;6(17):15412–15419. doi:10.1021/am503909q